IEEE Access
Multidisciplinary | Rapid Review | Open Access Journal

Received 16 May 2023, accepted 1 June 2023, date of publication 7 June 2023, date of current version 23 June 2023.

Digital Object Identifier 10.1109/ACCESS.2023.3283299

RESEARCH ARTICLE

Optimal Fuzzy Wavelet Neural Network Based Road Damage Detection

MOHAMMAD ALAMGEER[1], HEND KHALID ALKAHTANI[2], MASHAEL MAASHI[3], MAHMOUD OTHMAN[4], ANWER MUSTAFA HILAL[5], MOHAMED IBRAHIM ALSAID[5], AZZA ELNEIL OSMAN[5], AND AMANI A. ALNEIL[5]

[1]Department of Information Systems, College of Science and Art at Mahayil, King Khalid University, Muhayil Assir 61421, Saudi Arabia
[2]Department of Information Systems, College of Computer and Information Sciences, Princess Nourah bint Abdulrahman University, Riyadh 11671, Saudi Arabia
[3]Department of Software Engineering, College of Computer and Information Sciences, King Saud University, Riyadh 11543, Saudi Arabia
[4]Department of Computer Science, Faculty of Computers and Information Technology, Future University in Egypt, New Cairo 11835, Egypt
[5]Department of Computer and Self Development, Preparatory Year Deanship, Prince Sattam bin Abdulaziz University, Alkharj 16273, Saudi Arabia

Corresponding author: Anwer Mustafa Hilal (a.hilal@psau.edu.sa)

The authors extend their appreciation to the Deanship of Scientific Research at King Khalid University for funding this work through Large Groups Project under grant number (RGP2/134/44). Princess Nourah bint Abdulrahman University Researchers Supporting Project number (PNURSP2023R384), Princess Nourah bint Abdulrahman University, Riyadh, Saudi Arabia. Research Supporting Project number(RSPD2023R787), King Saud University, Riyadh, Saudi Arabia. This study is supported via funding from Prince Sattam bin Abdulaziz University project number (PSAU/2023/R/1444).

ABSTRACT Floods are one of the most severe and most frequent natural calamities. It causes enormous economic damage and even leads to higher mortality rates. Studies on damage detection of roads using artificial intelligence (AI) methods gained more attention currently, especially in the development of smart cities. Therefore, this study designs an optimal Fuzzy Wavelet Neural Network based Road Damage Detection (OFWNN-RDD) technique for Flooding Management. The OFWNN-RDD technique aims to exploit the remote sensing images to classify different kinds of roads. For noise removal process, the OFWNN-RDD technique utilizes Gabor filtering (GF) technique. In addition, the OFWNN-RDD technique uses the DenseNet121 model for feature vector generation with modified barnacles mating optimization (MBMO) based hyperparameter optimizer. Finally, FWNN image classification approach is used for road damage detection. The simulation values exhibit the supremacy of the OFWNN-RDD technique over other models with improved road damage detection accuracy of 98.56%.

INDEX TERMS Flooding, road damage, machine learning, parameter tuning, computer vision.

I. INTRODUCTION

Natural catastrophes, namely wildfires, floods, and earthquakes, cause huge losses to flatten buildings, and substructures and block roads, causing heavy economic and social losses [1]. Roads are regarded as lifelines. As soon as a disaster happened, road damage detection and valuation were the basis for emergency rescue operations. To assess, identify and detect road damage, several kinds of remote sensing (RS) data like Lidar and SAR, aerial or satellite images were widely utilized [2]. Mainly, high-resolution aerial images can be gained in a controlled way, concerning both flight planning and time and at radiometric, geometric and high spectral resolution to permit an emergency response [3]. This technique suits for a reliable and rapid post-disaster damages assessment since rapid accessibility and acquisition of images enable recognition of damaged road areas. Detecting injured roads over high-resolution aerial imagers can accelerate and enrich decision-making during a disaster [4].

Studies on artificial intelligence (AI) based road damage detection model has gained significant attention in the recent times [5]. Since manual road damage detection is a laborious and time consuming process, the automatic analysis and follow-up of road damages can be used [6]. Government agency cannot keep up an accurate database of the road conditions. Another problem is the short fall of professionals who could evaluate the spread and state of numerous damages, as the assessment will often be highly subjective [7].

Conventional techniques to collect samples in the domain are cost-intensive and time-consuming [8]. Thus, numerous

The associate editor coordinating the review of this manuscript and approving it for publication was Kathiravan Srinivasan.

research efforts were held to help government agency for automating the sample collection process and road inspection, using technology with various degrees of complexity. Current research works have implemented several Deep Learning (DL)-related and Machine Learning (ML) methods for automated damage detection or road surface survey [9]. DL, which depends on neural networks, will be an advanced conception of ML and grants solutions in application fields that are tough to model with classical statistical methods.

Convolutional Neural Networks (CNNs) are the main category of deep neural networks (DNNs) that can be generally implemented for image classification and recognition [10]. The main benefit of CNN is that it mechanically finds critical features after the training phase by not involving any human supervision. On the other hand, hyperparameters are settings that are not learned during training, but must be set prior to training. They can have a significant impact on the performance of the model, and selecting the optimal values can lead to better accuracy. Most of the existing works have not addressed the hyperparameter tuning process. Since the trial and error parameter tuning is a tedious process, metaheuristic optimization algorithms are preferable.

This study designs an optimal Fuzzy Wavelet Neural Network based Road Damage Detection (OFWNN-RDD) technique for Flooding Management. The OFWNN-RDD method uses Gabor filtering (GF) for noise removal. The OFWNN-RDD technique uses the DenseNet121 model for feature vector generation with hyperparameter tuning using the modified barnacles mating optimization (MBMO) algorithm. This study employs the FWNN image classification approach for road damage detection. A complete set of series was performed to highlight the proficient classification performance of the OFWNN-RDD algorithm. In short, the key contributions are summarized as follows.

- An intelligent OFWNN-RDD technique comprising of pre-processing, DenseNet121 based feature extraction, MBMO based hyperparameter tuning, and FWNN based classification is presented for road damage detection. To the best of our knowledge, the OFWNN-RDD model has never presented in the literature.
- A novel MBMO algorithm is introduced by incorporating the concepts of self-adaptive population into the BMO algorithm.
- Employ FWNN model for the identification and classification of road damage detection process.
- Hyperparameter optimization of the DenseNet121 model using MBMO algorithm using cross-validation helps to boost the predictive outcome of the OFWNN-RDD model for unseen data.

The rest of the paper is organized as follows. Section II provides the related works and section III offers the proposed model. Then, section IV gives the result analysis and section V concludes the paper.

II. RELATED WORKS

Al Duhayyim et al. [11] introduced a novel Road Damage Detection modality utilizing Hunger Games Search and Elman NN (RDD–HGSENN) on High-Resolution RSI. The RDD–HGSENN approach mainly intends to fix road destructions through RSIs. In the approach mentioned above, the RetinaNet method has been enforced to detect road damage. Besides, the RDD–HGSENN algorithm can categorise road damage through the ENN method. The HGS system has been used in this study for tuning ENN variables mechanically. Reference [12] presents a new method relevant to the Tracking, Learning, and Detector (TLD) structures for detecting the damaged road area from post-disaster high-resolution RSI. Initially, spoke wheel operators can be used to describe the initial template of the road. Afterwards, the TLD structure was exploited to find suspected road damaged regions. Lastly, damaged road parts were extracted by pruning false damaged roads.

Ochoa-Ruiz et al. [13] aim at bridging this gap through 2 methods. First, the author presented a novel large asphalt dataset, which incorporated damages not existing in earlier research works, making it very powerful and representative of some reimbursements like potholes. The images are captured in various weather and illumination circumstances, and a quality-aware data augmenting technique has been used for sorting out examples of bad quality, which will be helpful in enriching the performance metrics on the baseline. Then, the author well-trained various object detection methods agreeable for mobile applications with a suitable performance for several applications. Hacıefendioğlu and Başağa [14] concentrated on identifying cracks in concrete roads for several illumination levels, shooting and weather conditions utilizing a DL-related object detection technique. In this context, previous cracks will be determined unusually inexpensively and quickly. A descriptive method is taken into account for detecting cracks of images on concrete road surfaces utilizing pre trained Faster R-CNN.

Shim et al. [15] advanced a new sensor technology that finds road damage through a DL-relevant image processing technique. The presented technology is a semi-supervised learning and super-resolution method related to GAN. In the previous days, the quality of road image so that damages can be observed clearly. Such 2 techniques are allplied to 4 lightweight segmentation neural networks. Li et al. [16] modelled an automated common subsurface distress detection technique unitizing conventional deep learning and signal processing. Wavelet transform was enforced to find the road layer for function segmentations. A particular pseudo-color map technique was modlle4d for converting reflected signals for DL model training.

A novel large-scale manhole cover detection datasets are introduced utilizing smartphones for collecting road image datasets, and a hierarchical classification approach related to the CNN is devised in [17]. Wang et al. [18] introduced an improved approach depending on YoloV3 that considers

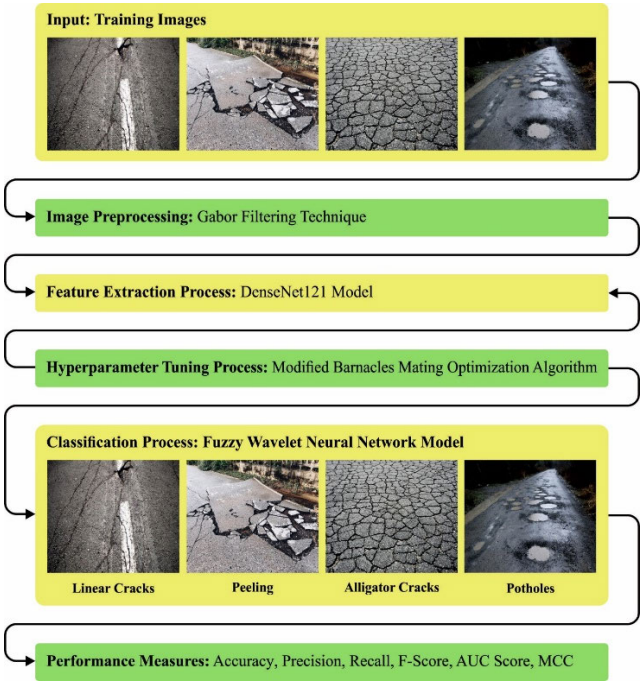

FIGURE 1. The overall workflow of OFWNN-RDD system.

the tininess nature and slenderness of the road damage that needed detailed and low-level description. Yuan et al. [19] introduced EcRD: an edge-cloud-related road damage detection and warning structure that uses the fast-responding advantages of edge and extensive computation resources and storage advantages of cloud. Samma et al. [20] intend to introduce a pre-trained VGG-19 leveraging a potential two-layer optimizer. The presented optimizer performed filter selection of the last layers of VGG-19 guided by the precision of the linear SVM classifier. Gan et al. [21] develops one approach related to M2det that can derive the deep and shallow features. For its multi-level and multi-scale, it belongs to one-stage. The author used M2det for detecting road damage, training on a more image snapped by vehicle-mounted smartphones, and then comparing it with the other one-stage approaches.

III. THE PROPOSED MODEL

In this study, we have designed a novel OFWNN-RDD approach for road damage detection in Flooding Management. The OFWNN-RDD technique focused on the effectual classification of roads into different types. To accomplish this, the OFWNN-RDD technique comprises GF preprocessing, DenseNet121 feature extractor, MBMO hyperparameter tuning, and FWNN-based classification. Fig. 1 shows the overall workflow of OFWNN-RDD system. Initially, the proposed model receives the road images as input and then eliminate the noise exist in it using the GF based preprocessing technique. Next, the DenseNet121 model extracts a useful set of feature vectors and the MBMO algorithm is applied to optimally choose the DenseNet121 model. Finally, the FWNN model is exploited for road damage classification process.

A. DATA PREPROCESSING

Primarily, the OFWNN-RDD technique used the GF technique for the noise removal process. In the presented system, the Gabor filter (GF) was exploited to relax the valleys and enhance the ridges by implementing a short-term Fourier transformation involving a Gaussian window in the spatial domain [22]. This statistical feature produced an image feature emphasized by applying the orientations and frequency information in fingerprint images by finetuning GFs. A sequence of GFs is used on the image $I(x, y)$ in different frequencies, which have distinct orientations with $g(x, y)$ Gabor function as follows.

$$g(x, y) = \exp\left(-\frac{x'^2 + \gamma^2 y'^2}{2\sigma^2}\right)\cos\left(2\pi\frac{X'}{l} + \phi\right) \quad (1)$$

where, $\chi' = xcox\theta + ysin\theta$ and $y' = ycox\theta - xsin\theta$. This Gabor transform is employed on the Gaussian envelope σ along with χ and y directions.

B. FEATURE EXTRACTION

The OFWNN-RDD technique applied the DenseNet121 model for feature vector generation. CNN achieves superior performance in the image classification domain [23]. But training the CNN from scratch is difficult as the classification accuracy based on hyperparameter tunings such as initial weight, learning rate, optimizers, number of epochs, and dropout requires higher computation power and many labeled training datasets. These problems are leveraged by using TL technique. During the TL algorithm, training duration is minimalized by the weight accomplished from the pre-trained method that can be exploited as an initial weight to train the innovative difficulties. This technique of re-using pretrained weights outcomes in low generalization error. The DenseNet model is widespread because the DenseNet framework attenuates the gradient vanishing problems, stimulates feature reuse, enhances feature propagation, and decreases the parameter count. In DCNN, every layer was linked with the other layers as feed forward patterns. All the layers in DenseNet accept the feature mas of every preceding layer as another input and passed on the feature map to all the every layer. Hence, $n - th$ layers have n inputs of every layer.

Generally, CNN changes its feature map size through the downsampling layer. But DenseNet facilitates feature concatenation and downsampling by splitting the network into densely connected dense blocks. The size of feature maps in the block remains the same, and inside dense blocks, they assist to perform concatenation, whereas, outside dense blocks, convolution and pooling functions are implemented for down-sampling. A transition layer or block was added at the end of the dense layers. The transition layer includes 2×2 average pooling layers, a batch normalization layer, and a 1×1 convolutional. The transition layer will change

the feature map size. Hence, the DenseNet includes 3 transitions, 1-classification, and 117 Conv, which makes the size of layer 121.

In this work, the hyperparameter tuning process uses the MBMO algorithm. In this work, the MBMO technique as a hyperparameter optimizer has been employed. Barnacle is a specific type of arthropod that constitutes an infraclass Cirripedia depends on lobsters and crabs [24]. They are especially marine animals which live in shallow and tidal waters. They will be available everywhere one seawater and raised on hard surfaces in seawater. Afterwards, they hatch eggs; barnacle larvae were dispersed in water to discover and stick towards hard surfaces. The hard surface covers the body of the barnacle and improves the shell plate. They need to search for a balance between achieving additional mates in a turbulent flow and dealing with ever-longer penises. Depending on this behaviour, a new optimization approach, called the BMO algorithm, was proposed. The balance behaviors are developed by using Hardy Weinberg equilibrium in the following. The primary population of barnacles for the solution is defined as follows:

$$X = \begin{Bmatrix} \chi_1^1 & \chi_1^N \\ \vdots & \vdots \\ \chi_n^1 & \chi_n^N \end{Bmatrix} \tag{2}$$

In Eq. (2), n determines the candidate numbers, and N indicates the amount of decision variables based on the upper and lower limiations:

$$l_b = \left[l_b^1, \ldots, l_b^i\right] \tag{3}$$

$$u_b = \left[u_b^1, \ldots, u_b^i\right] \tag{4}$$

Now, u_b and l_b denote the upper and lower boundaries of parameter i. By evaluating the objective function for every candidate, best to worst upshots are arranged and stored during primary iteration. The proposed technique includes exploitation and exploration. The offspring generation is enforced using sperm cast as an exploration term:

$$b_D = rand\ (n) \tag{5}$$

$$b_M = rand\ (n) \tag{6}$$

From the expression, b_D and b_M indicates mated parents.

Based on Hardy Weinberg's concept, the BMO technique considers the inheritance feature or parents' genotype frequency during the generation of offspring for modelling the reproduction technique:

$$X_i^{N_{new}} = pX_{b_D}^N + qX_{b_M}^N \tag{7}$$

In Eq. (7), $X_{b_M}^N$ and $X_{b_D}^N$ correspondingly characterize the variable of Mum and Dad candidates, and p determines a pseudorandom number that lies within [0,1], $= (1-p)$.

Once the candidate selection to mate excels pl amount was initially considered, then exploration term is performed:

$$X_i^{N_{new}} = randd \times X_{b_M}^n \tag{8}$$

where *rand* describes the random number within [0, 1], the recently produced offspring for exploration is produced using Mum's candidates. The offspring would be evaluated and added to parents for extending the solution matrix from candidate size. Therefore, a method has been exploited to arrange a single dimension, eliminating incorrect solutions. The MBMO technique incorporates self-population-related initialization with the typical BMO technique. Like other metaheuristics, BMO has a population-related optimized algorithm initiated by random initialization. This shows that it demands control parameters for determining population sizes. Yet, it is notable that the selection of population sizes to overcome case problem become challenging. Here, the primary population size in the first iteration was attained using a self-adaptive population:

$$PopSize = 10 \times d \tag{9}$$

In Eq. (9), d denotes the problem dimension, and the following expression determines it:

$$PopSize_{new} = \max\left(d, round\left(PopSize + r \times PopSize\right)\right) \tag{10}$$

In Eq. (10), r determines a random value within [−0.5, 0.5].

Algorithm 1 Pseudocode of BMO

```
Initializes population of barnacle X_i
Evaluate the barnacle fitness valu
Sort for locating an optimal outcome at the population
(T=the optimal solutions)
  while (I < Maximal iteration)
  Fix values of pl
    if select of Dad and Mum =pl
      for every variable
      Offspring generations:
  end for
else if selective of Dad and Mum >pl
  for every variable
    Offspring generation
    End for
  end if
  Apply existing barnacle backs when it moves
outside the boundary
  Evaluate barnacle fitness valu
  Arrange and upgrade T when there was an
optimal solution
  l=l+1
end whil
Return T
```

The MBMO approach derived a fitness function to have an enriched classifier outcome. It determined positive values for signifying superior outcomes of candidate solutions. This article uses the reduced classifier error rate as the fitness

function, as offered in Eq. (11).

$$fitness\,(x_i) = ClassifierErrorRate\,(x_i) = \frac{number\ o\,fmisclassified\ samples}{Total\ number\ of\ samples} * 100 \quad (11)$$

C. CLASSIFICATION USING FWNN MODEL

For road damage detection, the FWNN image classification approach is employed in this work. For classification purposes, the proposed method integrates a WNN and FNN [25]. The network comprises eight levels based on the proposed method.

(1) First Layer. The input features are the initial layer of the projected FWNNet. They are Time series, Independent variables, and picture classification features.

$$X = \{X_j \,|\, j = 1, \ldots, n\} \quad (12)$$

(2) Second Layer. This layer encompasses WNN and FNN for the approximation. The wavelet is calculated through the wavelet portion:

$$\psi_{ij}^{k} = \psi\left(\frac{x_j - b_{ij}^{k}}{a_{ij}^{k}}\right), i = 1, \ldots, N, j = 1, \ldots, n \quad (13)$$

N indicates the number of wavelets, whereas n indicates the number of input features.

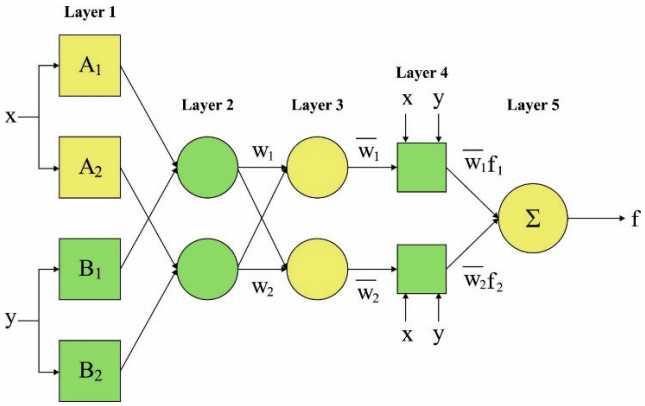

FIGURE 2. The architecture of FWNN.

Wavelet transformation, at the same time, display function and discloses its local features in the time-frequency domain. This feature makes it easy to train NN for accurately modelling tremendously non-linear data:

$$\psi_{a,b} = |a|^{-\left(\frac{1}{2}\right)} \psi\left(\frac{x-b}{a}\right), a, b \in R, a \neq 0, \quad (14)$$

In Eq. (14), $\psi(x) \in L^2(R)$ denotes the wavelet function as follows:

$$C_\psi = \int_0^{+\infty} \frac{|\hat{\psi}(\omega)|}{\omega} d\omega < +\infty. \quad (15)$$

In Eq. (15), $\hat{\psi}(\omega)$ denotes the FTs of $\psi(x)$. To stimulate multi-variable processes, a multidimensional wavelet should

TABLE 1. Details of dataset.

Class	No. of Sample Images
Linear Cracks	1000
Peeling	1000
Alligator Cracks	1000
Potholes	1000
Total Number of Sample Images	4000

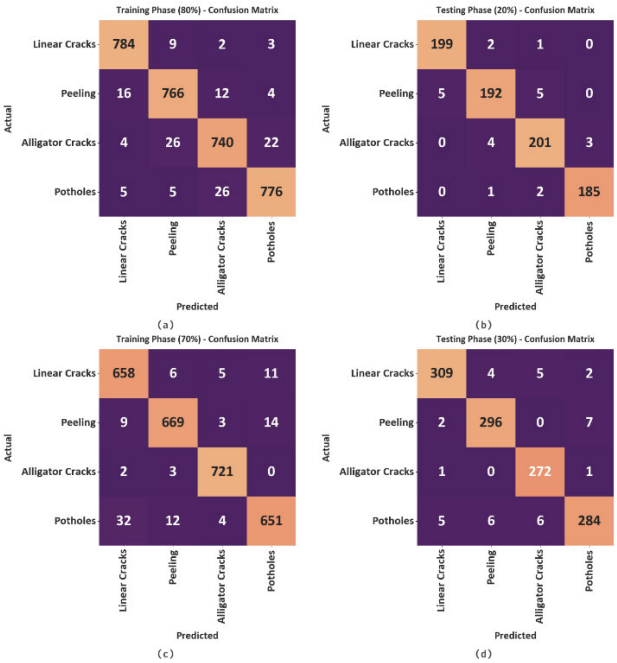

FIGURE 3. Confusion matrices of OFWNN-RDD approach (a-b) TRS/TSS of 80:20 and (c-d) TRS/TSS of 70:30.

be designed. Moreover, the fuzzy membership function is calculated in the fuzzy region of second layer as follows:

$$\mu_{kj} = e^{-((x_j - c_{kj})/\sigma_{kj})^2} \quad (16)$$

In Eq. (16), c_{kj} indicates the center, and σ_{kj} shows standard deviation for the rule k membership function. Fig. 2 illustrates the framework of FWNN.

(3) Third Layer. The third layer is the aggregation layer, where the output of layer 3 should be collectively multiplied. Multiple WNNs with N_k wavelet activation function are applied in the wavelet portion:

$$\Psi_i^k = \prod_{j=1}^{n} \psi^k ij, k, 1, \ldots, M \quad (17)$$

Moreover, each node in layer 3 demonstrates one fuzzy rule:

$$O_k = \prod_{j=1}^{n} \mu_{kj}, k, 1, \ldots, M \quad (18)$$

(4) Fourth Layer. The output of the wavelet component was calculated:

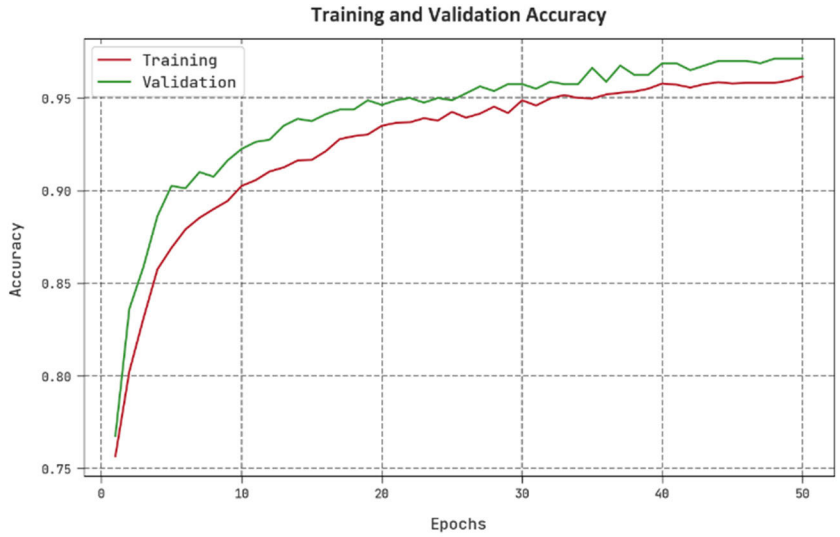

FIGURE 4. TACC and VACC outcome of OFWNN-RDD approach.

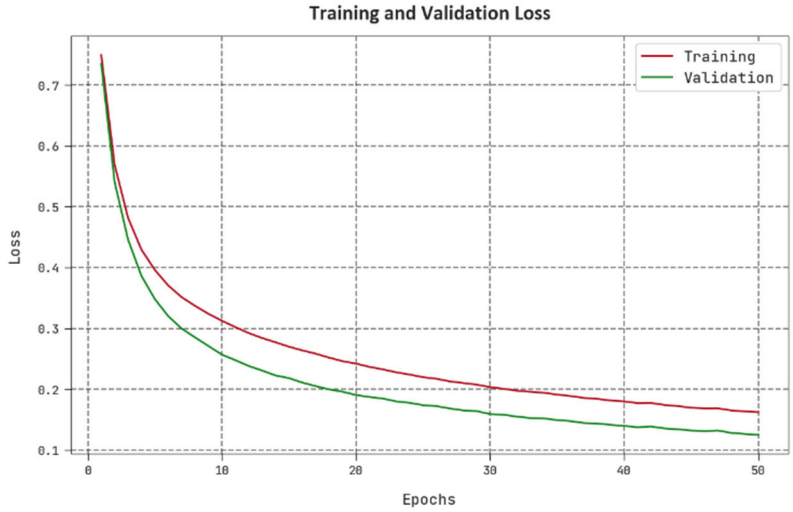

FIGURE 5. TLS and VLS outcome of OFWNN-RDD approach.

R_k : IF x_1 is A_{k1}... AND x_n is A_{kn},
THEN

$$Y_k = \sum_{i=1}^{N_k} w_i^k \Psi_i^k + \overline{y}_k \tag{19}$$

where $x_1, x_2, \ldots, x_n$ signify the input feature, $Y_1, Y_2, \ldots, Y_M$ characterizes the 4th layer resultant layer, and A_{kj} signifies the k^{th} fuzzy set with standard membership. The weight matrix and bias were saved in the hidden layer as w_i^k and $\overline{y}_k$.

(5) Fifth Layer. The results of FNN and WNN in the third and fourth layers, O_k and Y_k, are integrated. The defuzzification inference was s in this layer, and it multiplies the 3rd resultant layers dataset by the 4th resultant dataset.

(6) Sixth Layer. Two neurons correspondingly act as a summing operator for 5th and 3rd layer resultant signals. 7th layer output neurons produced the quotient that demonstrates every WNNs output is proportional to the FWNNet results.

$$\begin{aligned} O_k^{(5)} &= O_k^{(3)} \cdot O_k^{(4)} = O_k \cdot Y_k, \\ O_1^{(6)} &= \sum_{k=1}^{M} O_k^{(5)} \\ O_2^{(6)} &= \sum_{k=1}^{M} O_k^{(3)} \end{aligned} \tag{20}$$

(7) Seventh Layer. The result of the output is gathered at the 7th layer.

$$y = O^{(7)} = \frac{O_1^{(6)}}{O_2^{(6)}} = \frac{\sum_{k=1}^{M} O_k Y_k}{\sum_{k=1}^{M} O_k} \tag{21}$$

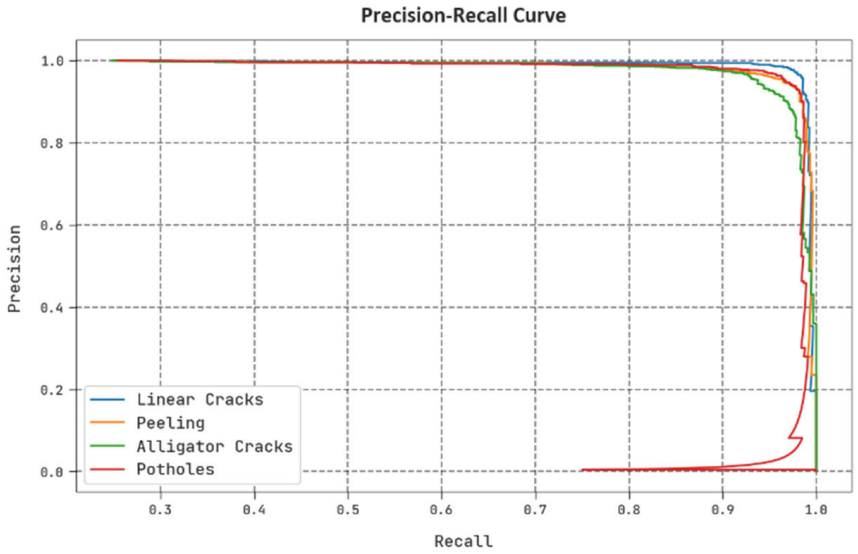

FIGURE 6. The precision-recall outcome of OFWNN-RDD approach.

TABLE 2. Road classifier outcome of OFWNN-RDD system under 70:30 of TRS/TSS.

Class	$Accu_y$	$Prec_n$	$Reca_l$	F_{score}	AUC_{score}	MCC
Training Phase (70%)						
Linear Cracks	97.68	93.87	96.76	95.29	97.37	93.77
Peeling	98.32	96.96	96.26	96.61	97.63	95.49
Alligator Cracks	99.39	98.36	99.31	98.83	99.37	98.43
Potholes	97.39	96.30	93.13	94.69	95.97	92.99
Average	98.20	96.37	96.37	96.36	97.58	95.17
Testing Phase (30%)						
Linear Cracks	98.42	97.48	96.56	97.02	97.83	95.94
Peeling	98.42	96.73	97.05	96.89	97.97	95.83
Alligator Cracks	98.92	96.11	99.27	97.67	99.04	96.98
Potholes	97.75	96.60	94.35	95.46	96.62	93.98
Average	98.38	96.73	96.81	96.76	97.86	95.68

TABLE 3. Road classifier outcome of OFWNN-RDD method under 80:20 of TRS/TSS.

Class	$Accu_y$	$Prec_n$	$Reca_l$	F_{score}	AUC_{score}	MCC
Training Phase (80%)						
Linear Cracks	98.78	96.91	98.25	97.57	98.60	96.76
Peeling	97.75	95.04	95.99	95.51	97.16	94.01
Alligator Cracks	97.12	94.87	93.43	94.15	95.89	92.25
Potholes	97.97	96.40	95.57	95.98	97.18	94.62
Average	97.91	95.80	95.81	95.80	97.21	94.41
Testing Phase (20%)						
Linear Cracks	99.00	97.55	98.51	98.03	98.84	97.36
Peeling	97.88	96.48	95.05	95.76	96.94	94.35
Alligator Cracks	98.12	96.17	96.63	96.40	97.64	95.14
Potholes	99.25	98.40	98.40	98.40	98.96	97.91
Average	98.56	97.15	97.15	97.15	98.09	96.19

8) Eighth Layer. This was the network layer for feature classification. It can be an activation function which transforms data into output layer value.

IV. EXPERIMENTAL VALIDATION

The proposed model is simulated using Python 3.6.5 tool. The proposed model is experimented on PC i5-8600k, GeForce 1050Ti 4GB, 16GB RAM, 250GB SSD, and 1TB HDD. The parameter settings are given as follows: learning rate: 0.01, dropout: 0.5, batch size: 5, epoch count: 50, and activation: ReLU.In this study, road damage classifier outcomes of the OFWNN-RDD technique can be tested using the dataset [11] comprising 4000 samples with 4 class labels, as represented in Table 1.

The road damage identification outcomes of the OFWNN-RDD method are investigated under distinct aspects in the form of a confusion matrix in Fig. 3. The results deliberated that the OFWNN-RDD process has recognized four types of road damage accurately.

Table 2 reports the overall road classifier outcomes of the OFWNN-RDD method with 70:30 of TRS/TSS. On 70% of TRS, the results indicated that the OFWNN-RDD technique has proficiently categorized four types of road damage. It is observable that the OFWNN-RDD technique reaches average $accu_y$ of 98.20%, $prec_n$ of 96.37%, $reca_l$ of 96.37%, $F_{score}$of 96.36%, AUC_{score} of 97.58%, and MCC of 95.17%.

Table 3 offers the overall road classification outcomes of the OFWNN-RDD system with 80:20 of TRS/TSS. On 80% of TRS, the results exhibited the road classifier outcome of the OFWNN-RDD method with 80% of TRS. The results indicated that the OFWNN-RDD system has proficiently categorized four types of road damage. It is observable that the OFWNN-RDD technique reaches average $accu_y$ of 97.91%,

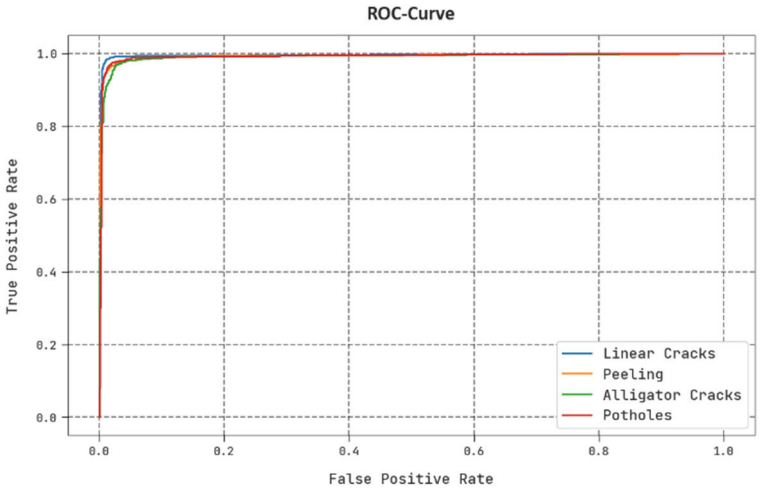

FIGURE 7. ROC curve outcome of OFWNN-RDD approach.

TABLE 4. Comparative analysis of OFWNN-RDD methodology with other techniques.

Methods	$Accu_y$	$Prec_n$	$Reca_l$	F_{score}
OFWNN-RDD	98.56	97.15	97.15	97.15
RDD-HGSENN	98.03	96.25	96.34	96.29
AlexNet	92.84	93.52	93.83	92.95
GoogleNet	91.47	92.23	91.33	91.39
RetinaNet	90.70	89.45	89.80	90.17
MobileNet	90.03	90.88	88.97	89.15

$prec_n$ of 95.80%, $reca_l$ of 95.81%, F_{score} of 95.80%, AUC_{score} of 97.21%, and MCC of 94.41%.

The TACC and VACC of the OFWNN-RDD method are inspected on road classification performance in Fig. 4. The results pointed out that the OFWNN-RDD algorithm has exhibited enhanced outcomes with increased values of TACC and VACC. It is observable that the OFWNN-RDD system has reached superior TACC outcomes.

The TLS and VLS of the OFWNN-RDD system are tested on road classification performance in Fig. 5. The figure inferred that the OFWNN-RDD method had enhanced performance with the least values of TLS and VLS. It is perceptible that the OFWNN-RDD technique has resulted in lower VLS outcomes.

An evident precision-recall study of the OFWNN-RDD methodology in the test database is shown in Fig. 6. The results implied that the OFWNN-RDD system has led to superior values of precision-recall values in four class labels.

A comprehensive ROC study of the OFWNN-RDD method in the test database is exposed in Fig. 7. The outcomes indicated that the OFWNN-RDD algorithm had revealed its ability to classify four class labels.

A widespread comparison study of the OFWNN-RDD technique is briefed in Table 4 [11], [13]. The resultant values inferred the betterment of the OFWNN-RDD technique over other models. It is noticed that the RetinaNet and MobileNet models have obtained lower classifier outcomes. Next, the AlexNet and GoogleNet models have reached slightly enhanced performance. In contrast, the RDD-HGSENN technique has ensured reasonable performance with $anaccu_y$ of 98.03%. However, the OFWNN-RDD technique surpassed recent DL models with a maximum $accu_y$ of 98.56%. These results guaranteed the maximum performance of the OFWNN-RDD technique on the road classification process.

V. CONCLUSION

In this study, we have designed a new OFWNN-RDD technique for road damage detection in Flooding Management. The OFWNN-RDD technique focused on the productive classification of roads into different types. The OFWNN-RDD technique used the GF technique for noise removal to accomplish this. The OFWNN-RDD technique applied the DenseNet121 model for feature vector generation with hyperparameter tuning using the MBMO algorithm. This study employs the FWNN image classification approach for road damage detection. A complete set of experiments were performed to highlight the proficient classification performance of the OFWNN-RDD method. The simulation values demonstrate the supremacy of the OFWNN-RDD algorithm over other models with maximum accuracy of 98.56%. In future, the performance of the OFWNN-RDD method will be enhanced by the ensemble learning process.

ACKNOWLEDGMENT

The authors extend their appreciation to the Deanship of Scientific Research at King Khalid University for funding this work through Large Groups Project under grant number (RGP2/134/44). Princess Nourah bint Abdulrahman University Researchers Supporting Project number

(PNURSP2023R384), Princess Nourah bint Abdulrahman University, Riyadh, Saudi Arabia. Research Supporting Project number(RSPD2023R787), King Saud University, Riyadh, Saudi Arabia. This study is supported via funding from Prince Sattam bin Abdulaziz University project number (PSAU/2023/R/1444).

REFERENCES

[1] S. Shim, J. Kim, S.-W. Lee, and G.-C. Cho, "Road surface damage detection based on hierarchical architecture using lightweight auto-encoder network," *Autom. Construction*, vol. 130, Oct. 2021, Art. no. 103833.

[2] M.-T. Cao, Q.-V. Tran, N.-M. Nguyen, and K.-T. Chang, "Survey on performance of deep learning models for detecting road damages using multiple dashcam image resources," *Adv. Eng. Informat.*, vol. 46, Oct. 2020, Art. no. 101182.

[3] P. Hruza, T. Mikita, N. Tyagur, Z. Krejza, M. Cibulka, A. Procházková, and Z. Patočka, "Detecting forest road wearing course damage using different methods of remote sensing," *Remote Sens.*, vol. 10, no. 4, p. 492, Mar. 2018.

[4] M. Azimi, A. Eslamlou, and G. Pekcan, "Data-driven structural health monitoring and damage detection through deep learning: State-of-the-art review," *Sensors*, vol. 20, no. 10, p. 2778, May 2020.

[5] D. Arya, H. Maeda, S. K. Ghosh, D. Toshniwal, A. Mraz, T. Kashiyama, and Y. Sekimoto, "Deep learning-based road damage detection and classification for multiple countries," *Autom. Construct.*, vol. 132, Dec. 2021, Art. no. 103935.

[6] H. Maeda, Y. Sekimoto, T. Seto, T. Kashiyama, and H. Omata, "Road damage detection using deep neural networks with images captured through a smartphone," 2018, *arXiv:1801.09454*.

[7] M. Guerrieri and G. Parla, "Flexible and stone pavements distress detection and measurement by deep learning and low-cost detection devices," *Eng. Failure Anal.*, vol. 141, Nov. 2022, Art. no. 106714.

[8] C. Chu, L. Wang, and H. Xiong, "A review on pavement distress and structural defects detection and quantification technologies using imaging approaches," *J. Traffic Transp. Eng.*, vol. 9, no. 2, pp. 135–150, Apr. 2022.

[9] C. Dewi, R.-C. Chen, and H. Yu, "Weight analysis for various prohibitory sign detection and recognition using deep learning," *Multimedia Tools Appl.*, vol. 79, nos. 43–44, pp. 32897–32915, Nov. 2020.

[10] B. Abu-Salih, P. Wongthongtham, K. Coutinho, R. Qaddoura, O. Alshaweesh, and M. Wedyan, "The development of a road network flood risk detection model using optimised ensemble learning," *Eng. Appl. Artif. Intell.*, vol. 122, Jun. 2023, Art. no. 106081.

[11] M. Al Duhayyim, A. A. Malibari, A. Alharbi, K. Afef, A. Yafoz, R. Alsini, O. Alghushairy, and H. Mohsen, "Road damage detection using the hunger games search with Elman neural network on high-resolution remote sensing images," *Remote Sens.*, vol. 14, no. 24, p. 6222, Dec. 2022.

[12] K. Zhao, J. Liu, Q. Wang, X. Wu, and J. Tu, "Road damage detection from post-disaster high-resolution remote sensing images based on TLD framework," *IEEE Access*, vol. 10, pp. 43552–43561, 2022.

[13] G. Ochoa-Ruiz, A. A. Angulo-Murillo, A. Ochoa-Zezzatti, L. M. Aguilar-Lobo, J. A. Vega-Fernández, and S. Natraj, "An asphalt damage dataset and detection system based on RetinaNet for road conditions assessment," *Appl. Sci.*, vol. 10, no. 11, p. 3974, Jun. 2020.

[14] K. Hacıefendioğlu and H. B. Başağa, "Concrete road crack detection using deep learning-based faster R-CNN method," *Iranian J. Sci. Technol., Trans. Civil Eng.*, vol. 46, no. 2, pp. 1621–1633, Apr. 2022.

[15] S. Shim, J. Kim, S.-W. Lee, and G.-C. Cho, "Road damage detection using super-resolution and semi-supervised learning with generative adversarial network," *Autom. Construct.*, vol. 135, Mar. 2022, Art. no. 104139.

[16] Y. Li, C. Liu, G. Yue, Q. Gao, and Y. Du, "Deep learning-based pavement subsurface distress detection via ground penetrating radar data," *Autom. Construct.*, vol. 142, Oct. 2022, Art. no. 104516.

[17] B. Zhou, W. Zhao, W. Guo, L. Li, D. Zhang, Q. Mao, and Q. Li, "Smartphone-based road manhole cover detection and classification," *Autom. Construct.*, vol. 140, Aug. 2022, Art. no. 104344.

[18] Q. Wang, J. Mao, X. Zhai, J. Gui, W. Shen, and Y. Liu, "Improvements of YOLOv3 for road damage detection," *J. Phys., Conf. Ser.*, vol. 1903, no. 1, Apr. 2021, Art. no. 012008.

[19] Y. Yuan, M. S. Islam, Y. Yuan, S. Wang, T. Baker, and L. M. Kolbe, "EcRD: Edge-cloud computing framework for smart road damage detection and warning," *IEEE Internet Things J.*, vol. 8, no. 16, pp. 12734–12747, Aug. 2021.

[20] H. Samma, S. A. Suandi, N. A. Ismail, S. Sulaiman, and L. L. Ping, "Evolving pre-trained CNN using two-layers optimizer for road damage detection from drone images," *IEEE Access*, vol. 9, pp. 158215–158226, 2021.

[21] X. Gan, J. Qu, J. Yin, W. Huang, Q. Chen, and W. Gan, "Road damage detection and classification based on M2det," in *Advances in Artificial Intelligence and Security*. Dublin, Ireland: Springer, Jul. 2021, pp. 429–440.

[22] A. A. Albraikan, M. Aljebreen, J. S. Alzahrani, M. Othman, G. P. Mohammed, and M. I. Alsaid, "Modified barnacles mating optimization with deep learning based weed detection model for smart agriculture," *Appl. Sci.*, vol. 12, no. 24, p. 12828, Dec. 2022.

[23] T. Chauhan, H. Palivela, and S. Tiwari, "Optimization and fine-tuning of DenseNet model for classification of COVID-19 cases in medical imaging," *Int. J. Inf. Manage. Data Insights*, vol. 1, no. 2, Nov. 2021, Art. no. 100020.

[24] A. M. Agwa, S. K. Elsayed, and E. E. Elattar, "Extracting the parameters of three-diode model of photovoltaics using barnacles mating optimizer," *Symmetry*, vol. 14, no. 8, p. 1569, Jul. 2022.

[25] M. Ahmadi, F. D. Ahangar, N. Astaraki, M. Abbasi, and B. Babaei, "FWNNet: Presentation of a new classifier of brain tumor diagnosis based on fuzzy logic and the wavelet-based neural network using machine-learning methods," *Comput. Intell. Neurosci.*, vol. 2021, Nov. 2021, Art. no. 8542637.